Supplementary Information

Significantly shorter Fe-S bond in cytochrome P450-I is consistent with greater reactivity relative to chloroperoxidase

Courtney M. Krest,[a] Alexey Silakov, Jonathan Rittle, Timothy H. Yosca, Elizabeth L. Onderko, Julio C. Calixto, and Michael T. Green*

Department of Chemistry, Penn State University, University Park, PA 16802

[a]Current address: Stanford Synchrotron Radiation Lightsource, SLAC National Accelerator Laboratory, Menlo Park, California, 94025

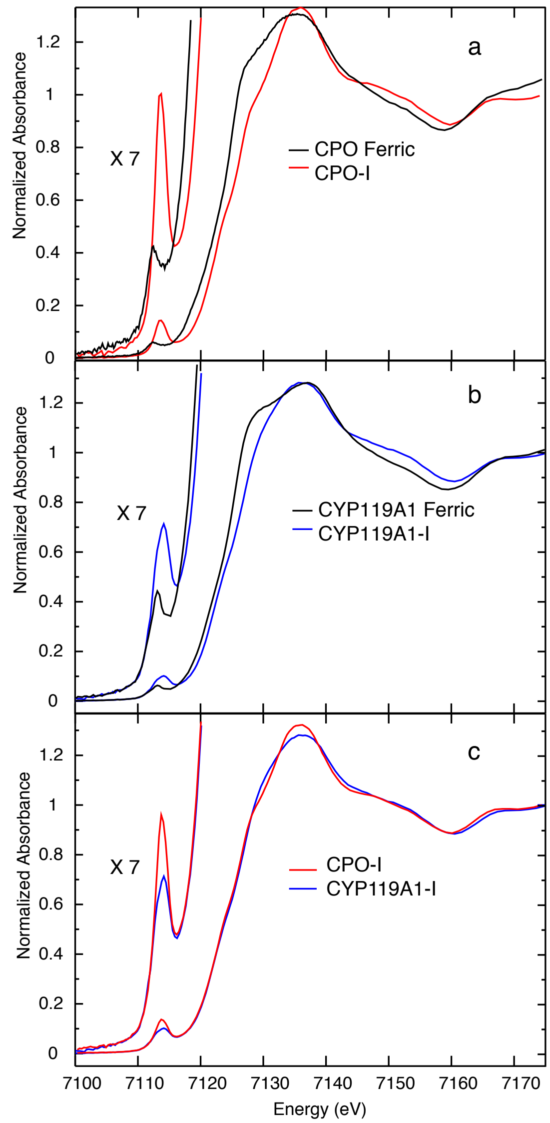

Figure S1. Fe K-edge XANES region showing the rising edge with the pre-edge expanded by a factor of 7. a) CPO ferric (blue), CPO-I (red). b) CYP119A1 ferric (blue), CYP119A1-I (black). c) Comparison of the XANES of both compound I species, CPO-I (red) CYP119A1-I (black).

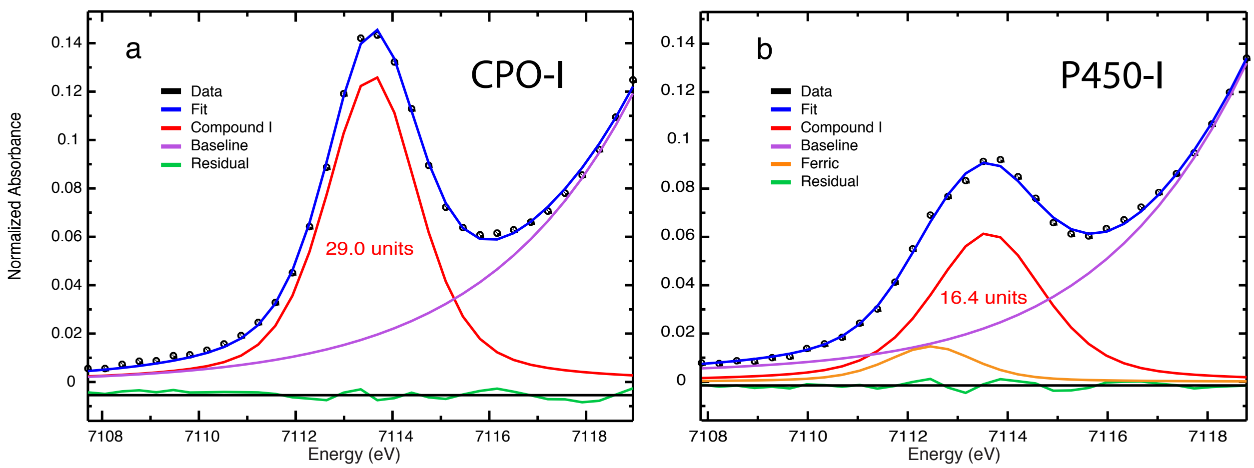

Figure S2. Representative pre-edge fits. Fits of the pre-edge data indicate that the CPO-I pre-edge (a) is 14±8 % larger than the CYP119A1-I pre-edge (b). Fits of P450-I data accounted for the contribution of ~30% ferric enzyme. To obtain the final pre-edge area for P450-I, the value obtained from the fit must be scaled by 1.43 (i.e. 1.0/0.7).

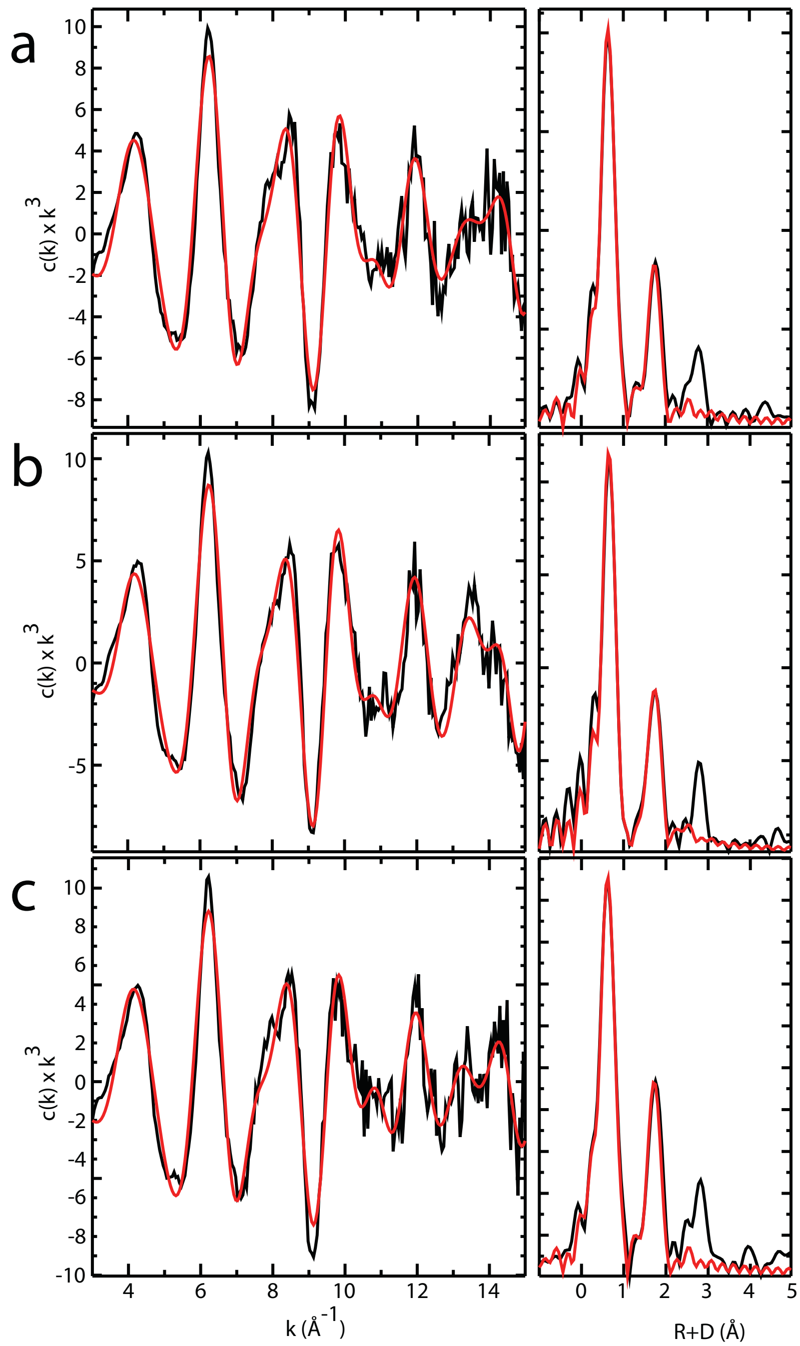

Figure S3. EXAFS and Fourier transforms for ferric P450 119A1(a), 158A2(b), and 119A2(c).

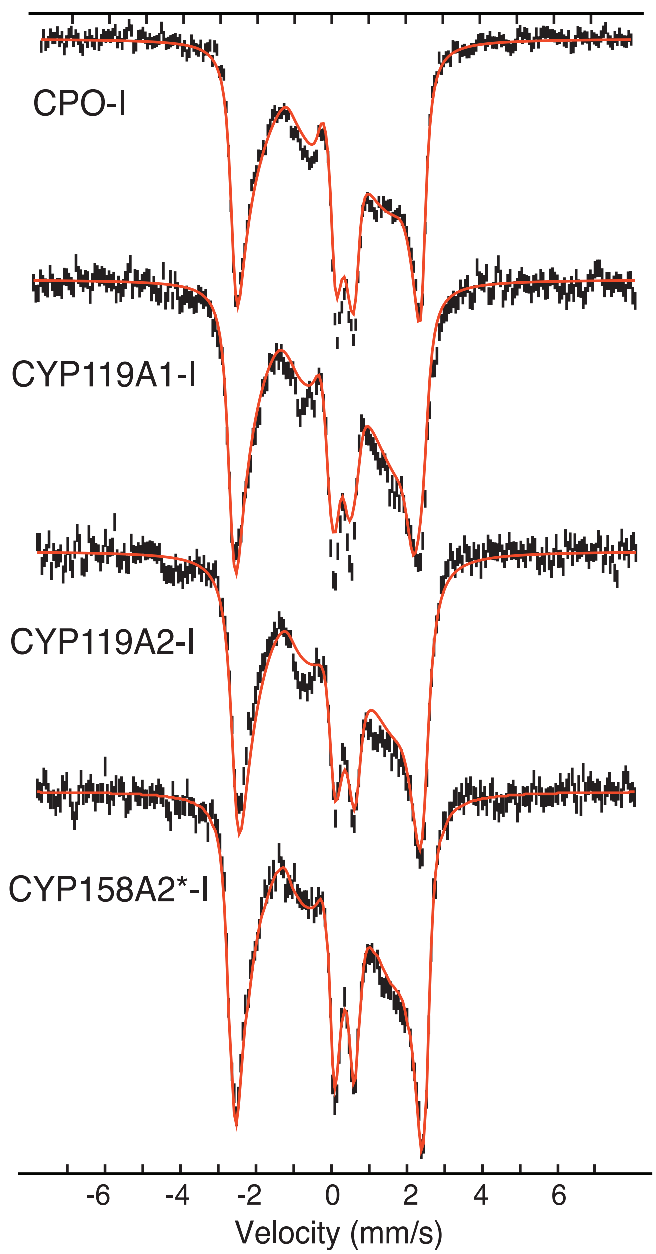

Figure S4. Mössbauer spectra of compound I at 4.2 K with 54-mT field applied parallel to the γ-beam. To obtain the P450-I spectra, contributions from ferric enzyme were subtracted from the raw data.

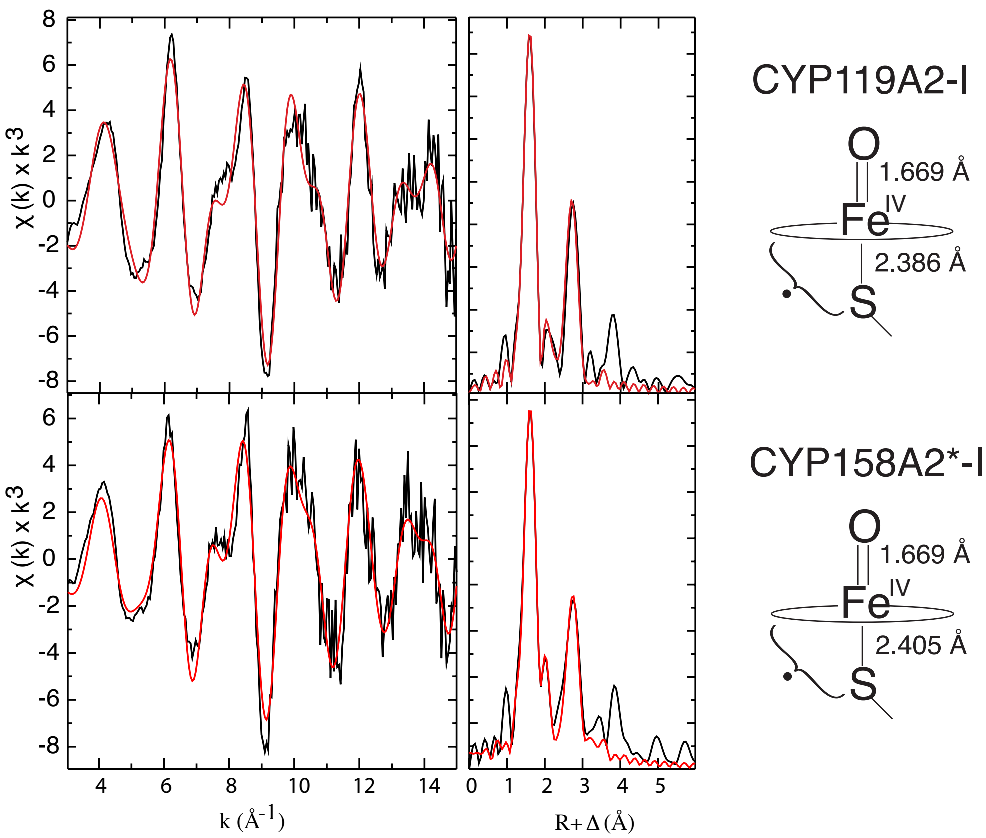

Figure S5. EXAFS and Fourier transforms for CYP119A2-I and CYP158A2*-I.

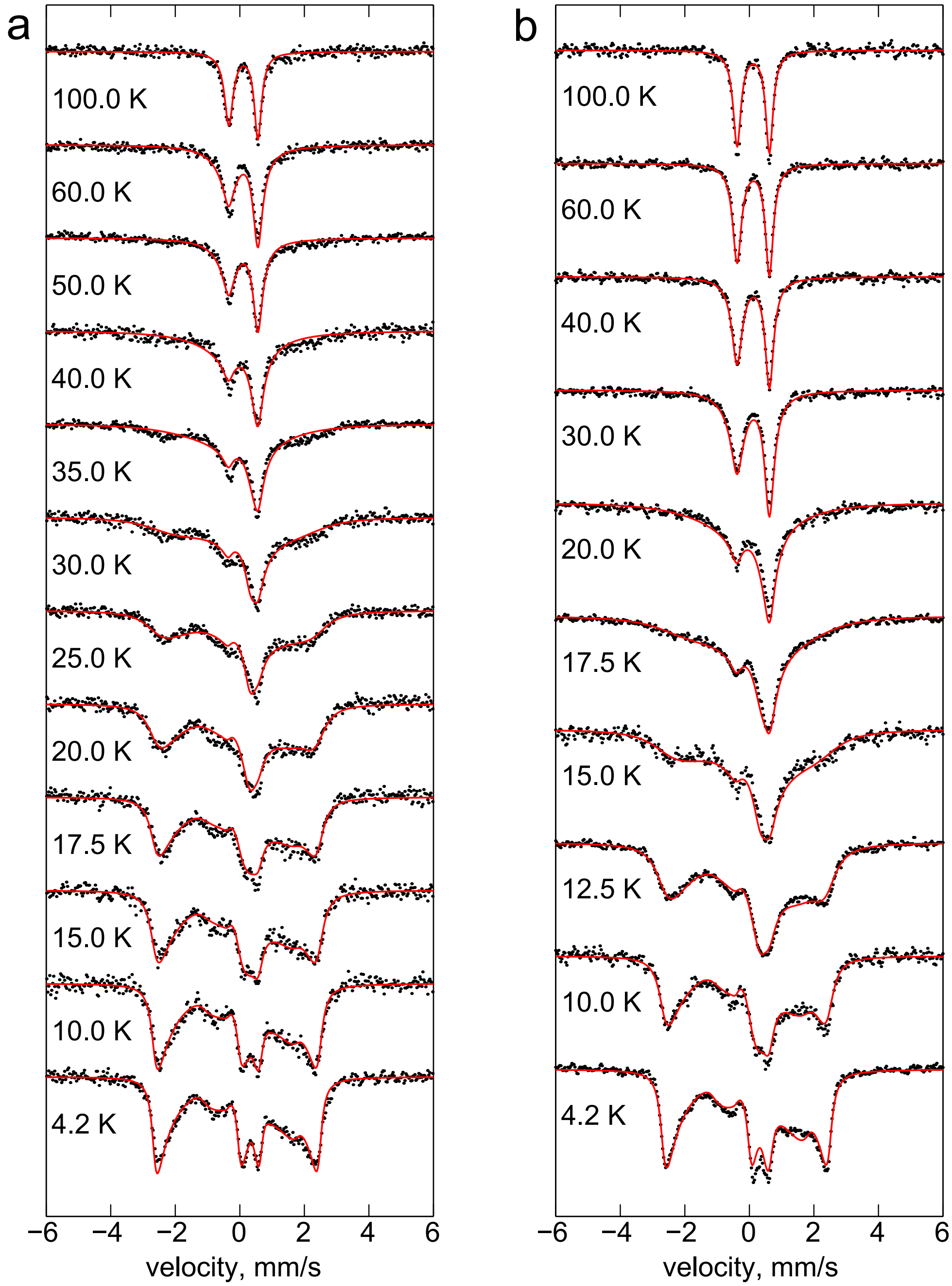

Figure S6. Variable temperature Mössbauer data and fits for CYP119A1-I (a) and CPO-I (b). To obtain the CYP119A1-I spectra, contributions from ferric enzyme (Fig. S4) were subtracted from the raw data. A 54-mT field was applied parallel to the γ-beam. Note that the Mössbauer spectrum of ferric CYP119A1 was found to be independent of temperature below ~ 40K. As a result, the 15K and 17.5K CYP119A1-I spectra were obtained by subtracting the 10K ferric spectrum from the raw data, while the 25K CYP119A1-I spectrum was obtained by subtracting the 20K ferric spectrum.

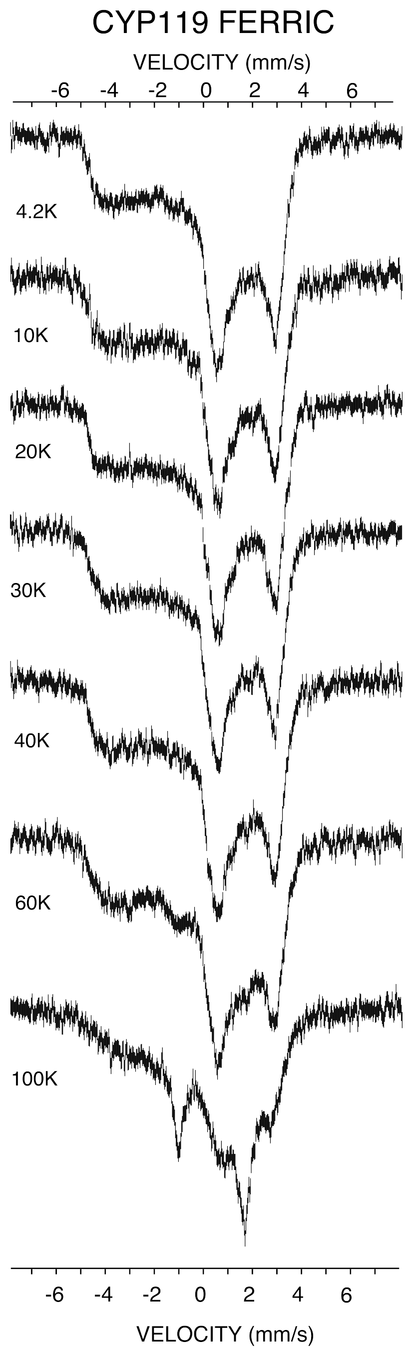

Figure S7. Variable temperature Mössbauer data for ferric CYP119A1. A 54-mT field was applied parallel to the γ-beam.

Table S1. Ground-state (S=1/2) Mössbauer parameters used to simulate spectra presented in Figure 3 and S6.

	δ (mm/s)	ΔE$_Q$ (mm/s)	g$_x$	g$_y$	g$_z$	A$_x$ (T)	A$_y$ (T)	A$_z$ (T)	FWHH* (mm/s)
CPO-I	0.13	0.96	1.72	1.61	2.00	-31	-30	-2	0.32
CYP119-I	0.11	0.90	1.96	1.86	2.00	-28	-32	-3	0.25

* - FWHH stands for Full Width at Half Height of Lorentzian lineshape.

Table S2. Temperature dependent relaxation parameters used for simulating Mössbauer spectra presented in Figure 3 and S6.

Temp. (K)	**Relaxation parameter (x10^6 s^{-1})**			
	CYP119-I		**CPO -I**	
	trial 1	**trial 2**	**trial 1**	**trial 2**
10.0	2.41	2.31	9.29	2.62
12.5	-	-	17.87	18.44
15.0	5.54	6.52	50.82	47.32
17.5	8.14	-	87.79	-
20.0	14.55	17.24	148.02	146.37
25.0	34.77	-	-	-
30.0	86.75	73.43	659.20	698.21
35.0	137.37	-	-	-
40.0	174.05	200.33	1548.31	1922.99
50.0	493.54	-	-	-
60.0	446.16	451.16	3777.46	7069.86
100.0	2783.31	1358.13	7735.16	18771.33

Table S3. Best fits for ferric P450 EXAFS data. Each row corresponds to a best fit for data obtained from measurements on an independently prepared set of samples.

	Fe-N			Fe-S				
	N	R	σ^2	N	R	σ^2	E_0	Error
CYP119A1	4	1.994	0.0011	1	2.219	0.0013	-15.1	0.294
	4	1.990	0.0013	1	2.212	0.0014	-16.2	0.471
	4	1.990	0.0011	1	2.216	0.0013	-19.0	0.299
	4	1.991	0.0014	1	2.210	0.0013	-16.0	0.327
Average		**1.992**			**2.214**			
90% Conf. Interval		**0.002**			**0.005**			
CYP158A2*	4	2.005	0.0009	1	2.2131	0.0025	-14.1	0.272
CYP119A2	4	1.987	0.0014	1	2.2121	0.0014	-16.8	0.338
Avg. (all P450s)[a]		**1.997**			**2.212**			
90% Conf. Interval		**0.009**			**0.004**			

[a]Average includes the distance obtained previously for ferric $P450_{cam}$. (Ref. 3 of main text.)

Optimized coordinates for calculations

All geometry optimization calculations were performed in Gaussian 03[1] with the B3LYP[2] functional, TZVP[3] basis set, and COSMO[4] with the dielectric for water. The Fe-S and Fe-O bonds were constrained to the experimental determined distances during geometry optimizations. Protoporphyrin IX was modeled as porphine ligand. Cysteine was modeled as a methyl thiolate ligand. Spectral calculations were done with ORCA. First using ORCA 2.8[5] a single point calculation was done using the optimized geometry from Gaussian, the B3LYP[2] functional, TZVP[2] basis set, and COSMO[4] with a dielectric of water. Next TD-DFT calculations were done in ORCA with the same geometry, using the previous B3LYP[2] result as an initial guess, the BP86[6, 7] functional, TZVP basis set, and COSMO[4] with a dielectric of water, as well as core properties basis set, CP(PPP),[8] on the Fe atom. Plots of the results were made using the orca_mapspc feature in ORCA and orbitals were visualized using orca_plot.[5] Input files for pre-edge feature prediction were based on input files from Chandrasekaran *et al*.[9]

CYP119-I

Geometry used for pre-edge calculation. Geometry was optimized with Fe-S and Fe-O distances constrained to the values obtained from EXAFS measurements.

N	1.154797	1.735783	-0.137600
C	2.511543	1.835373	-0.004675
C	2.902711	3.220352	0.052806
C	1.763348	3.953437	-0.050020
C	0.676200	3.015930	-0.165527
C	3.396147	0.767303	0.069014
C	3.051992	-0.571486	-0.008597
C	3.990967	-1.663390	0.020907
C	3.268486	-2.806254	-0.106751

C	1.884620	-2.417425	-0.203635
N	1.775961	-1.055033	-0.140126
C	0.824372	-3.306471	-0.320122
C	-0.511740	-2.958614	-0.360745
C	-1.604743	-3.891909	-0.450772
C	-2.749834	-3.163484	-0.478329
C	-2.367509	-1.775856	-0.413029
N	-1.001377	-1.671497	-0.323650
C	-3.245996	-0.707884	-0.469124
C	-2.890939	0.635296	-0.449408
C	-3.829904	1.725435	-0.521442
C	-3.105307	2.872486	-0.461684
C	-1.721938	2.486208	-0.353280
N	-1.617018	1.118819	-0.341457
Fe	0.086216	0.043043	-0.361904
O	0.186962	0.036458	-2.028849
C	-0.661570	3.371614	-0.266213
S	-0.042105	-0.330976	2.005298
C	-1.695646	0.049849	2.666591
H	-1.683320	-0.142819	3.738388
H	-1.965355	1.085327	2.467180
H	-2.436292	-0.605131	2.202273
H	-3.457069	3.892513	-0.485974
H	-4.899554	1.609054	-0.604505
H	-4.300513	-0.938401	-0.550813
H	-3.767998	-3.515307	-0.544471
H	-1.491235	-4.964541	-0.487630

H	1.064505	-4.360980	-0.364554
H	3.621491	-3.825917	-0.128748
H	5.059443	-1.551127	0.123126
H	4.446994	1.002928	0.178949
H	3.919185	3.567437	0.158186
H	1.650999	5.026773	-0.045401
H	-0.894840	4.428639	-0.274837

CPO-I

Geometry used for pre-edge calculation. Geometry was optimized with Fe-S and Fe-O distances constrained to the values obtained from EXAFS measurements.

N	1.153056	1.730718	-0.129348
C	2.509895	1.831017	0.007733
C	2.899822	3.215992	0.070429
C	1.760726	3.948778	-0.036180
C	0.674428	3.011301	-0.158405
C	3.395513	0.764286	0.076700
C	3.051651	-0.573919	-0.008633
C	3.991499	-1.664989	0.016892
C	3.270223	-2.807990	-0.116083
C	1.886325	-2.419921	-0.212434
N	1.775798	-1.057635	-0.143047
C	0.827141	-3.309428	-0.329920
C	-0.508825	-2.961061	-0.365244
C	-1.601369	-3.894584	-0.451201
C	-2.747058	-3.166684	-0.472226
C	-2.365506	-1.779336	-0.407615
N	-0.998299	-1.673637	-0.323466

C	-3.245907	-0.713279	-0.458954
C	-2.891112	0.629332	-0.440286
C	-3.830319	1.719274	-0.508816
C	-3.105687	2.866488	-0.453666
C	-1.721905	2.480926	-0.350701
N	-1.616177	1.113105	-0.337868
Fe	0.087931	0.039499	-0.376309
O	0.192220	0.044341	-2.023003
C	-0.662517	3.367148	-0.264486
S	-0.058124	-0.359423	2.056884
C	-1.702894	0.070987	2.707938
H	-1.680230	-0.050659	3.790379
H	-1.975185	1.090364	2.442545
H	-2.447817	-0.615518	2.298495
H	-3.457712	3.886458	-0.476587
H	-4.900376	1.602624	-0.585978
H	-4.300477	-0.944740	-0.536480
H	-3.765371	-3.518930	-0.533828
H	-1.487432	-4.967118	-0.489678
H	1.067305	-4.363734	-0.377996
H	3.623970	-3.827325	-0.141286
H	5.059712	-1.552161	0.121268
H	4.446102	1.000087	0.188396
H	3.915740	3.563076	0.181245
H	1.647896	5.022065	-0.029669
H	-0.895900	4.424075	-0.275919

References

1. Frisch, M. J.; Trucks, G. W.; Schlegel, H. B.; Scuseria, G. E.; Robb, M. A.; Cheeseman, J. R.; Montgomery, J., J. A.; Vreven, T.; Kudin, K. N.; Burant, J. C.; Millam, J. M.; Iyengar, S. S.; Tomasi, J.; Barone, V.; Mennucci, B.; Cossi, M.; Scalmani, G.; Rega, N.; Petersson, G. A.; Nakatsuji, H.; Hada, M.; Ehara, M.; Toyota, K.; Fukuda, R.; Hasegawa, J.; Ishida, M.; Nakajima, T.; Honda, Y.; Kitao, O.; Nakai, H.; Klene, M.; Li, X.; Knox, J. E.; Hratchian, H. P.; Cross, J. B.; Bakken, V.; Adamo, C.; Jaramillo, J.; Gomperts, R.; Stratmann, R. E.; Yazyev, O.; Austin, A. J.; Cammi, R.; Pomelli, C.; Ochterski, J. W.; Ayala, P. Y.; Morokuma, K.; Voth, G. A.; Salvador, P.; Dannenberg, J. J.; Zakrzewski, V. G.; Dapprich, S.; Daniels, A. D.; Strain, M. C.; Farkas, O.; Malick, D. K.; Rabuck, A. D.; Raghavachari, K.; Foresman, J. B.; Ortiz, J. V.; Cui, Q.; Baboul, A. G.; Clifford, S.; Cioslowski, J.; Stefanov, B. B.; Liu, G.; Liashenko, A.; Piskorz, P.; Komaromi, I.; Martin, R. L.; Fox, D. J.; Keith, T.; Al-Laham, M. A.; Peng, C. Y.; Nanayakkara, A.; Challacombe, M.; Gill, P. M. W.; Johnson, B.; Chen, W.; Wong, M. W.; Gonzalez, C.; Pople, J. A. *Gaussian 03*, Revision E.01; Gaussian, Inc.: Wallingford, CT, 2004.
2. Devlin, F.; Finley, J.; Stephens, P.; Frisch, M., Ab Initio Calculation of Vibrational Absorption and Circular Dichroism Spectra Using Density Functional Force Fields: A Comparison of Local, Nonlocal, and Hybrid Density Functionals *J. Phys. Chem.* **1995,** *99*, 16883-16902.
3. Schafer, A.; Huber, C.; Ahlrichs, R., Fully optimized contracted Gaussian basis sets of triple zeta valence quality for atoms Li to Kr. *J. Chem. Phys.* **1994,** *100* (8), 5829-5835.
4. Klamt, A.; Schuurmann, G., COSMO: a new approach to dielectric screening in solvents with explicit expressions for the screening energy and its gradient. *J. Chem. Soc. Perk. Trans.* **1993,** *2* (5), 799-805.
5. Neese, F. *ORCA an Ab Initio, Density Functional, and Semiempirical Electronic Structure Program Package*, Version 2.8; Universitat Bonn, Germany, 2011.
6. Becke, A., Density-functional exchange-energy approximation with correct asymptotic behavior. *Phys Rev A* **1988,** *38* (6), 3098-3100.
7. Perdew, J., Density-functional approximation for the correlation energy of the inhomogeneous electron gas. *Physical Review B, Condensed Matter* **1986,** *33* (12), 8822-8824.
8. Neese, F., Prediction and interpretation of the 57Fe isomer shift in Mössbauer spectra by density functional theory. *Inorganica Chimica Acta* **2002,** *337*, 181-192.
9. Chandrasekaran, P.; Stieber, S. C. E.; Collins, T. J.; Lawrence Que, J.; Neese, F.; DeBeer, S., Prediction of high-valent iron *K*-edge absorption spectra by time-dependent Density Functional Theory. *Dalton Transactions* **2011,** *40*, 11070-11079.